Wetting Phase Disintegration and Detachment: Three-Dimensional Confocal Imaging of Two-Phase Distributions

Parisa Bazazi,[1,2] Amir Sanati-Nezhad,[2,3] and Seyed Hossein Hejazi[1,*]

[1] *Porous Media Laboratory, Chemical and Petroleum Engineering, University of Calgary, Calgary, Alberta, Canada T2N 1N4*

[2] *BioMEMS and Bioinspired Microfluidic Laboratory, Department of Mechanical and Manufacturing Engineering, University of Calgary, Calgary, Alberta, Canada T2N 1N4*

[3] *Centre for Bioengineering Research and Education, University of Calgary, Calgary, Alberta, Canada T2N 1N4*

(Received 2 August 2018; revised manuscript received 20 November 2018; published 22 January 2019)

Three-dimensional (3D) confocal imaging of multiphase flows in a network of microcapillaries is used to conceptualize and quantify the mobilization process of an oleic wetting viscous phase by aqueous nanofluids and surfactant solutions. This microscale visualization reveals that nanoparticles decrease the thickness of wetting-phase film. The efficiency of surfactants in oil mobilization results from their capability to break the wetting phase into smaller ganglia. The type of injectant significantly influences the size of the clusters and the distribution of the wetting phase. We show that the mean size of the wetting phase clusters is a decreasing function of the displacement efficiency for each solution. Incorporation of silica nanoparticles with surfactant solutions hinders the wetting phase break up and decreases the number of clusters. The most frequently occurring cluster size (mode) decreases in the presence of surfactants, but remains unchanged in the presence of silica nanoparticles. Unlike the average cluster size, which is a decreasing function of the nonwetting phase saturation, it is interesting that the mode remains almost unchanged during the displacement process. The reduction of wetting film thickness and the fragmentation of wetting phase have numerous applications in natural and engineering sciences.

DOI: 10.1103/PhysRevApplied.11.014042

I. INTRODUCTION

Mobilization of a viscous phase by a less viscous fluid occurs in many naturally occurring situations and engineering processes. In particular, fluid-fluid-solid interfaces emerge in subsurface flow systems such as oil recovery, carbon dioxide sequestration, and soil remediation. The interface evolution is further affected when surface-active materials or suspended particles exist in the system.

The dynamics of two-phase flow in subsurface porous media is dependent on the surface and interfacial energies between solid surfaces and immiscible fluids. These energies control the efficiency of the displacement processes in porous medium flows. Oil recovery from petroleum reservoirs, carbon dioxide (CO_2) sequestration, groundwater treatment, soil remediation, and fuel cells can all be impacted [1–6]. During water-based viscous (heavy) oil displacement, a significant portion of oil remains unrecovered due to trapped oil ganglia and uneven displacements from the capillary force, medium heterogeneity, and oil-water viscosity mismatch. The extraction of oil from heavy crude oil deposits is limited by low fluid mobility at reservoir conditions and the strong affinity between the oil and solid surfaces in oil-wet rocks.

Polymers, surfactants, and alkalines are fed into the injected water to control the oil-water mobility and capillary pressure and decrease the residual oil saturation [7,8]. These chemicals alter solid surface wettability, increase injected phase viscosity, and decrease the interfacial energies between oil and water [9–11]. Nanoscale materials in the form of solid particles or aqueous suspensions (nanoparticles dispersed in water) have the potential to improve subsurface displacement processes [12–14]. Numerous studies demonstrate the potential of surface-treated titanium oxide [15] and metallic [16] and silica nanoparticles [17] for heavy crude oil recovery. Controlled microscale experiments demonstrate the success of nanoparticles in creating structural disjoining pressure [18,19]. Core-scale experiments of incremental oil recovery using nanoparticles is largely determined by changes in macroscopic properties such as interfacial tension and wettability [20–23]. The opacity of subsurface rocks in standard core-flood experiments obstructs the direct visualization of the fluid-fluid interfacial evaluation that governs the two-phase flow dynamics. Opacity

*shhejazi@ucalgary.ca

also hinders detailed characterization of the physics that underlies the nanofluid-oil displacement process in porous media. Therefore, the dynamics of fluid-fluid-solid interactions is obstructed in the presence of nanoparticles, surfactants, and polymers.

Over the past few years, the details of pore-scale displacement processes and the related mechanisms of snap-off, Hainse jump, the effect of wetting heterogeneities, and residual phases patterns have been captured by new art microfluidic technology and x-ray micro-CT scan imaging [4,24–28]. Additionally, microfluidics has provided the opportunity for engineering the two-phase flow in small scales [29,30]. In visualization studies, an overview of the flow process is recorded using two dimensional (2D) optical and fluorescence microscopy in the x-y plane [31–40]. The images captured represent the interactions between the fluids and solid surface in one focal plane where the aspects of the fluid interfaces in the third dimension are overlaid. The 3D imaging capability of x-ray micro-CT is limited by the scanning time. Hence, the images are not real-time and are often recorded after the experiment time scale [4,25]. Advances in confocal imaging have enabled physical discovery in different focal planes of the flow experiments where the 3D fluid displacement in porous media is visualized [41–44]. These studies improved understanding of porous medium flows at actual depths [39]; however, the role of chemical additives in the microscale dynamics of fluid-fluid-solid interactions in porous materials has received less attention. In particular, the fate of a continuous wetting phase when encountered with a less viscous fluid in the absence and presence of interfacial materials in the form of surface active agents and nanoparticles is not understood.

In this work, a 3D confocal imaging technique is used to quantify the size and shape of the wetting phase remaining after the injection of a nonwetting phase in combination with surfactants and nanoparticles into a network of interconnected microcapillaries. Spatiotemporal displacement of a wetting phase (viscous oil) with different displacing fluid compositions: deionized (DI) water, untreated silica nanoparticles, sodium dodecyl sulfate (SDS), polysorbate 20 (Tween 20), and trisiloxane (Silwet) surfactants are analyzed. The effect of nanoparticles and surfactants on the removal of a wetting phase film from the solid surfaces, wetting phase break up, and dynamics of phase interferences are systematically investigated. This work is a report on capturing and quantifying the interactions of nonionic surfactant molecules and silica particles and their combinations at the flowing fluid-fluid interfaces in a network of capillaries. We present three-dimensional (3D) observations of previously undefined immiscible viscous fluid-fluid displacement in the presence of surfactants and nanoparticles. The characterization of multiphase flows in a network of microcapillaries reveals that the mechanisms underlying the fluid-fluid displacement with nanoparticles

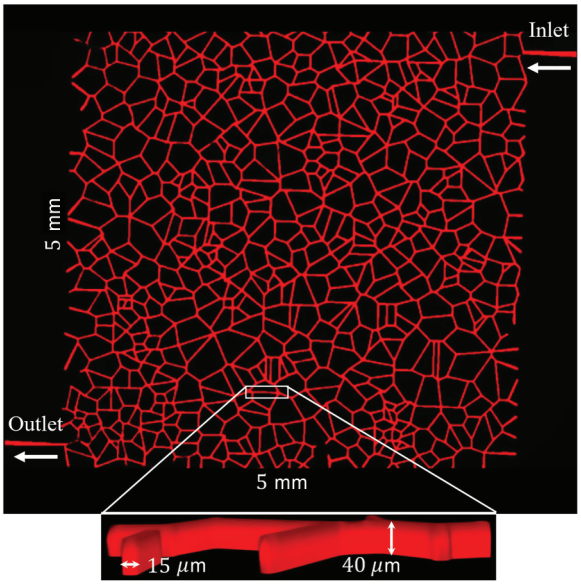

FIG. 1. 2D image of the microfluidic micromodel filled with mineral oil dyed using red fluorescent color. The magnified 3D images are shown for one microchannel with a depth and width of 40 and 15 μm, respectively. The fluid is injected through the top right inlet and is collected at the bottom left outlet.

are completely different from surfactant mechanisms. The outcome of this work is to recommend a complex fluid (i.e., a mixture of nanoparticles and surfactants) in the nonwetting phase. The complex fluid is applied to decrease the thickness of the remaining viscous wetting phase on the solid walls and fragment the wetting phase ganglia into many smaller parts.

II. EXPERIMENTAL SETUP

The experimental setup is designed to record visual spatiotemporal events during multiphase flow within microfluidic devices. Figure 1 illustrates a top view image of the network of microcapillaries made of polydimethylsiloxane (PDMS) material with a depth and width of 40 and 15 μm, respectively. The microreservoir network is composed of interconnected microchannels based on the design of Voronoi tessellation [45]. The fluid volume of the micromodel is 0.22 ± 0.05 μl. There is an average of 40 microchannels in each direction with an average length of 200 μm.

The microfluidic devices are placed horizontally on the stage of an inverted Nikon A1R microscope. The pressure-flow rate system (Fluigent) controls the fluid flow injection into the microfluidic device. The color (DS-RI2) and fluorescence camera [Zyla 4.2 PLUS sCM(OS)] are used to monitor fluid displacement and mixing. Actual 3D images of the fluid distribution within the microchannels are captured using confocal microscopy (red laser with a wavelength of 561 nm). Images are captured using long

working distances of ×2, ×10, and ×20 Nikon lenses. Displacement experiments are conducted by injecting an aqueous phase into a micromodel presaturated with heavy mineral oil. The oil is slowly injected into the channel network using a syringe pump connected to the micromodel with 1/8 in. tubing (Cole-Parmer). The oil-saturated micromodel is placed on the microscope stage and the aqueous phase is injected into the micromodel at a constant flow rate of 0.01 ml/h. In each experiment, the displacing fluid is injected from the top right corner and the fluids are produced from the bottom left corner (Fig. 1). Images of the flow displacement and fluid-fluid interactions are recorded at a variety of resolutions using a red excitation fluorescence filter at a rate of 100 frames per second. The images are saved as TIFF files and ImageJ [46] is employed for image analysis. The oil phase is shown in red and the aqueous phase is transparent. To distinguish the phases, a white color is assigned to the aqueous phase during the image processing step. Each experiment is repeated at least three times to validate the reliability of the data produced.

The microchannels are prefilled with mineral oil (Penarco: viscosity of 178 mPa s) and dyed with red fluorescent color (Kingscote-Mfr#506250-RF4). The fluorescent dye has no influence on the interfacial tension between the water and mineral oil. The aqueous phases used to displace oil are (i) DI water, (ii) three suspensions of 1, 2, and 4 wt. % silica, (iii) three solutions of 0.5 critical micelle concentration (CMC) Tween 20, Silwet, and SDS, and (iv) three mixtures of 2 wt. % silica and 0.5 CMC Tween 20, Silwet, and SDS. For the sake of brevity, these aqueous phases are respectively referred to as water (for DI water), Silica 1, Silica 2, and Silica 4 (for each silica suspension), Tween, Silwet, SDS (for surfactant solutions), and Tween-Silica, Silwet-Silica, and SDS-Silica (for mixtures). See the Supplemental Material at (URI) for the details of materials, microchip fabrication, and properties of oil and aqueous phases (interfacial tension and three-phase contact angle data) [47].

III. RESULTS AND DISCUSSION

The displacement of the wetting phase by the spread of displacing fluids (water, silica suspension, and surfactant solutions) is analyzed using 3D confocal images. The results reveal the dominant mechanisms of oil displacement subject to different displacing nanofluids and surfactant solutions alone or in combination.

A. Displacement performance

1. Sweep efficiency

Figure 2 illustrates a time series for the displacement of the wetting phase by DI water. The images are dedicated to different time points, including when water reaches the outlet [breakthrough time (t_{BT})] and two consecutive dimensionless times, $t_d = 2$ and 4. Dimensionless time is evaluated based on the volumetric flow rate (Q_{inj}) and the total volume of the network (V) defined as $t_d = (Q_{inj}t)/V$. The injected water follows the pathway with the least resistance between the injection and production ports (Fig. 2). Following the time t_{BT}, a larger number of microchannels are water invaded. The wetting phase at $t_d = 4$ is displaced through most microchannels at the central section of the fluidic network. For comparison, the overall pattern of wetting phase displacement at t_{BT} using Silica 1, 2, and 4 suspensions as well as Tween, Silwet, SDS solutions, and Tween-Silica, Silwet-Silica, and SDS-Silica mixtures are illustrated in Fig. 2. The results indicate that displacing silica tends to increase the uniform distribution of water. The overall displacement patterns for displacing silica are similar to those of water. Surfactant solutions change the displacement pattern; the Silwet forms a stable front attenuating the channeling effect. Similar to silica suspensions, the surfactant-silica mixture channels have greater invasion than the DI water channels.

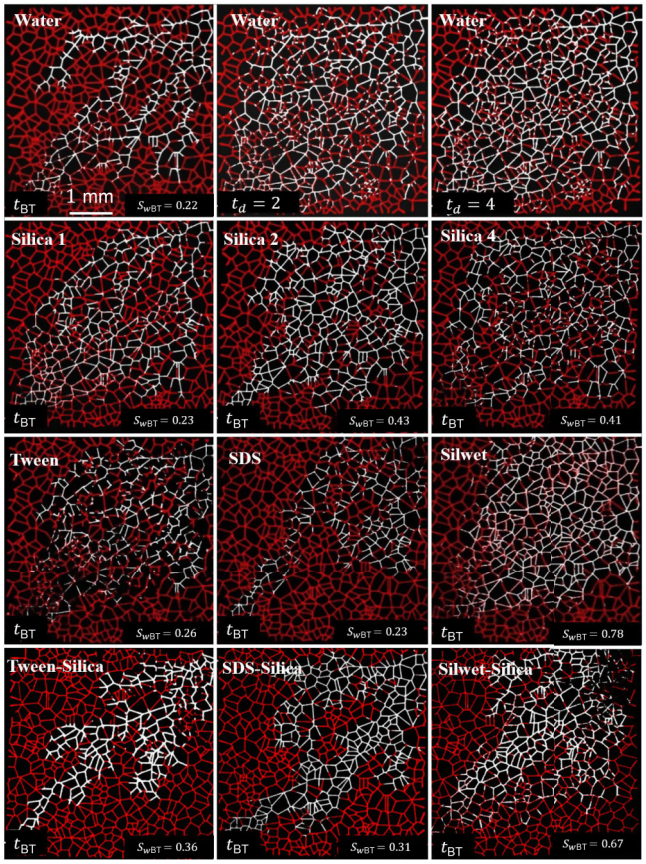

FIG. 2. 2D images of the aqueous phase-oil displacement through the microchannels' network by DI water, displacing fluids of silica suspensions, Tween, Silwet, SDS solutions, Tween-Silica, Silwet-Silica, and SDS-Silica mixtures. S_{WBT} is the water saturation evaluated based on the areal sweep and defined as the breakthrough time.

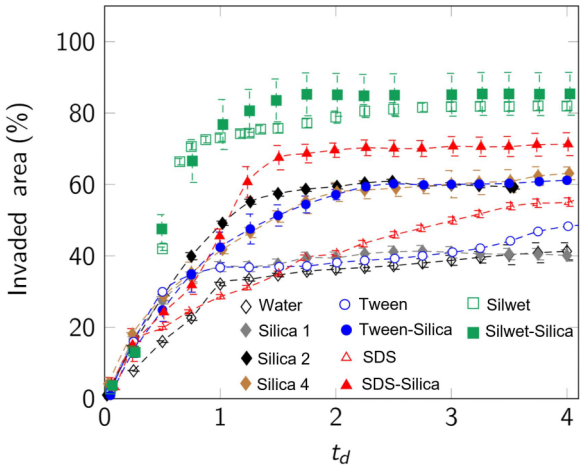

FIG. 3. Invaded area as a function of the dimensionless time for the oil displacement with DI water, silica suspensions, surfactant solutions, and silica-surfactant mixtures.

The efficiency of each fluid in oil displacement is quantified by measuring the areal ratio of invaded microchannels (white) to the total area of microchannels, referred to as areal sweep efficiency. Figure 3 provides the sweep efficiency of water, silica suspensions, surfactant solutions, and surfactant-silica mixtures. The addition of surfactants to the water improves the wetting phase displacement to $52.7 \pm 0.2\%$ for Tween, $62.0 \pm 2.4\%$ for SDS, and $82.4 \pm 1.2\%$ for Silwet after $t_d = 4$. The sweep effiecncy curves follow two regimes. First, an early quick rise until breakthrough ($t_d < 1$) followed by a steep decline in growth where the aqueous phase reaches the outlet and the communication paths between the injection and production ports are established. The outcome reveals that the incorporation of surfactants, solid particles, or a combination of both increases the wetting phase displacement. Sweep effieceincy is an increasing function of silica nanoparticles. In each case, the coupled surfactant-silica results in a higher wetting phase displacement than silica alone. During the early stages, the slope of sweep efficiency for chemical flooding scenarios are higher than those of the DI water. The chemicals improve the mobilization of the viscous wetting phase. It is noted that the snapshots in Fig. 2 are the 2D images ($\times 2$ magnification) of the multiphase flows in microcapillaries. The higher resolution 3D images are necessary to observe the patterns of wetting and nonwetting phases inside microcapillaries and their localized interactions. In the following sections, we first discuss the effect of the silica nanoparticles on the wetting phase distribution and later we focus on the effect of silica-surfactant solutions.

B. Silica suspension and oil displacement

To analyze the effect of silica nanoparticles on the oil displacement, we take the enlarged 2D and 3D images of multiphase flow in capillaries using a $\times 20$ optical objective. Figure 4(a) shows 3D images and Fig. 4(b) shows 2D images of the micromodel flooded with water and Silica 1, 2, and 4 wt. %, respectively. For each flooding scenario, the oil is first removed from the main body of microchannels, leaving a layer of oil attached to the hydrophobic surface of the PDMS. This wetting phase film, the residual oil, is thick (up to 40% of the microchannel height) and immobile in water even at $t_d = 10$. A detailed examination of the images in Fig. 4(a) reveals that the addition of silica nanoparticles decreases the thickness of the wetting phase film. The residual film is removed from the channel surfaces in the presence of Silica 4 wt. %. The dark microchannels represent almost 100% displacement of the wetting phase from the invaded microchannels. We quantify the effect of silica concentration in mobilizing the residual oil by measuring the remaining oil thickness for 10 invaded microchannels at $t_d = 10$ and at the center region of the micromodel. The measured thickness (h) is normalized by the microchannel width (w) and plotted as the function of silica concentration in Fig. 4(c), left axis.

We measure the volume of the remaining oil films in the invaded channels using the 3D object counter plug-in of ImageJ. The measured volume is scaled by the micromodel pore volume and plotted as a function of silica concentration in Fig. 4(c), right axis. Similar to the thickness, the volume of remaining oil film decreases as the silica concentration increases. It is evident that the oil film thickness slightly decreases from water to the Silica 1 flooding scenario. Consistent with the sweep efficiency, the oil-film thickness is considerably reduced for Silica 2 and reaches almost zero for Silica 4. The silica nanoparticles used in this study are untreated and do not change the interfacial tension between fluids [see Fig. S1(a) within the Supplementary Material [47]]. The silica nanoparticles have the capability to change the surface wettability when they are placed at the solid-liquid-liquid interfaces [48]. At the three-phase (solid surface, oil, and water) contact line, nanoparticles in the aqueous phase arrange themselves in well-ordered layers [18,49] resulting in a structural disjoining pressure in the film.

The nanoparticle ordering near the confined region of three phases results in the structural disjoining pressure which consequently enhances the spreading of nanofluid film on solids [18,50]. Hence, the presence of silica particles in the displacing fluid promotes the spreading of the nanofluid and effectively removes the remaining viscous phase. Figure 4(d) is a schematic of the oil-film removal process in the presence of nanoparticles. At the initial time of fluid injection (up to breakthrough), the wetting phase displacement is dependent on the main flow pathways of the porous media that have a low resistance to fluid flows. The injected fluid flows mainly through these pathways with a slight invasion to neighboring microchannels. Following the breakthrough, the interaction between oil and

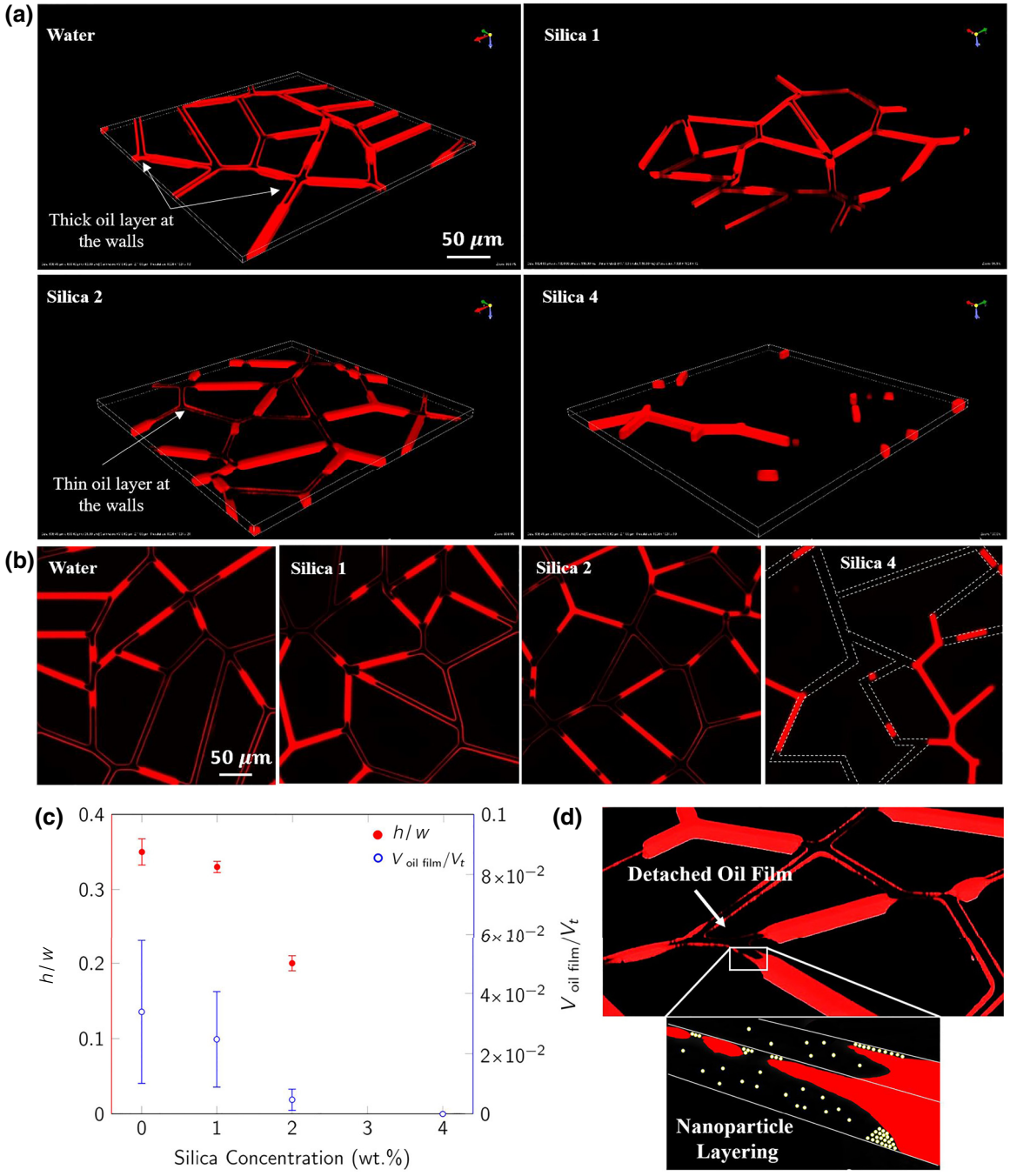

FIG. 4. The 2D and 3D images of the oil film layer and thickness and detachment mechanisms of the remaining wetting film in the micromodel flooded with water and different concentrations of silica nanoparticles. (a),(b), The effect of silica nanoparticles on the removal of the remaining wetting film from the solid surface at $t_d = 10$ of the water injection. (c) The dimensionless thickness and volume of the remaining wetting film, values to be read on the left and right axes, respectively. Increasing the silica concentration reduces the thickness and the volume of the oil films. (d) Schematic representation of the oil film removal in the presence of nanoparticles.

the displacing fluid is dominated by the mobilization of the residual wetting phase in the main flow pathways of the oil film and to a second degree to the invasion of new microchannels. For Silica 2 and 4 flooding when sufficient silica nanoparticles exist in the displacing fluid, nanoparticles play a key role in oil-film detachment. This ultimately results in an incremental improvement in the sweep efficiency postbreakthrough (Fig. 3).

The evaluation of the wetting phase film is illustrated at the inlet channel of the micromodel in Figs. 5(a) and 5(b) for the cases of water and Silica 4, respectively. For water, a thick layer of the wetting phase is attached to the wall,

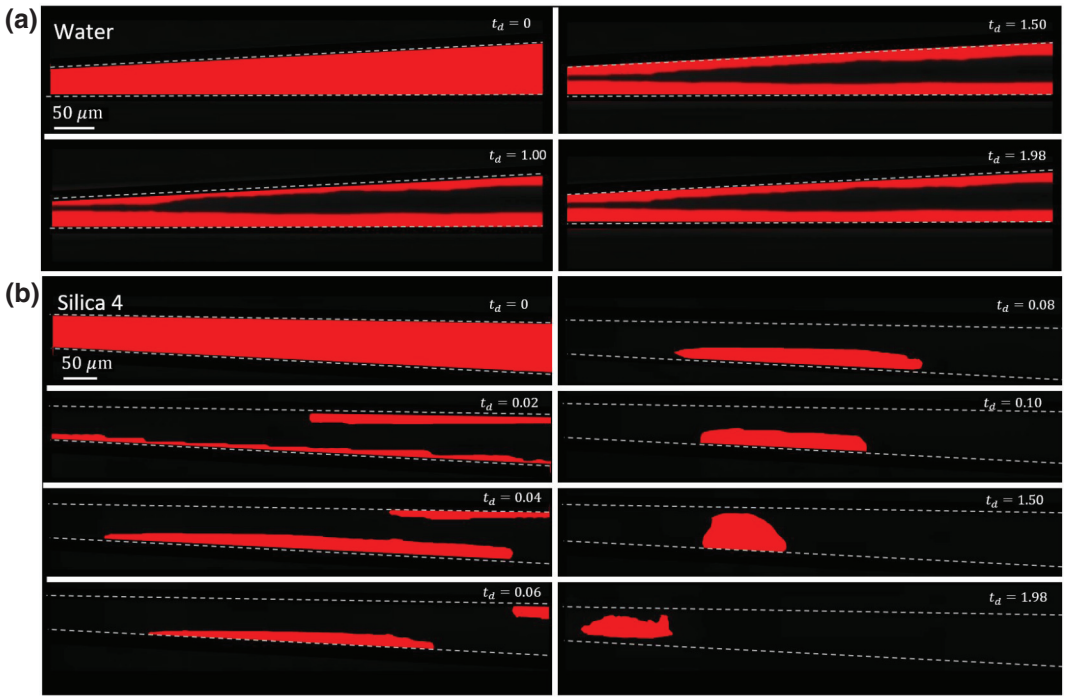

FIG. 5. The remaining wetting phase film at the entry channel of micromodel for (a) water and (b) Silica 4. (a) As the water injection continues, the film thickness is slowly reduced. (b) For Silica 4, the film thickness is much lower than that of water. The remaining wetting phase eventually gets detached in the form of a droplet.

where its thickness gradually decreases as the flow continues. When we inject Silica 4, the film thickness is lower than that of water, and the solid surface is quickly dewetted from the viscous phase. See the Supplemental Material at (URI) for the oil detachment by the silica nanoparticle suspension (see Movie S1 within the Supplementary Material) [47].

The effect of the surfactants on the wetting phase displacement is discussed in the next section.

C. 3D fluid distributions within microcapillaries

Following the exposure of microchannels to nonwetting phases, 3D images ($\times 10$ objective) of the multiphase flow within microcapillaries are taken from the center region of the micromodel network. The 3D images taken from water, Silica 2, Silica 4, Tween, SDS, Silwet, and silica-surfactant flooding experiments at $t_d = 10$ are shown in Fig. 6(a), where the remaining oil is shown in red color. The residual oil from the water flooding is observed in the form of a continuous blob. However, the wetting phase inside the microchannels is not continuous in the presence of surfactants. Owing to the reduction in interfacial tension (IFT), the wetting phase is broken down into smaller droplets. The number and size of wetting phase blobs are dependent on the type of surfactants. Silwet surfactant creates many tiny oil droplets that can be carried by the nonwetting phase toward the production port (Sec. III D). One may ascribe the improved sweep efficiency as a result of surfactants to the disintegration of the wetting phase (Fig. 3) [51]. On the other hand, Silica 2 and Silica 4 show different sweeping patterns. The wetting phase is mainly continuous in Silica 2, but is broken in Silica 4. This is, however, counterintuitive as the effect of silica on the change in IFT between the fluids (for all examined concentrations) is shown to be trivial [see Fig. S1(a) within the Supplementary Material [47]]. The clusters are defined as the discontinuous remaining wetting phases, in the form of oil ganglia, which can be in the shape of spheres, capsules, cuboids, or connected oil phases in multichannels. Throughout this paper, we interchangeably use the terms clusters, blobs, and ganglia. The average cluster size for water and surfactant solution injection is measured using IMAGE J. The dimensionless cluster sizes [area of the cluster (A_c)/total area of the microchannel (A_t)] are presented in Fig. 6(b). The error bars represent the standard deviation of the cluster size. The results show that the addition of SDS and Silwet to the injected fluid decreases the size of the remaining oil clusters.

The volume of oil clusters is measured using 3D, $\times 2$ magnification images that capture the entire micromodel pattern. Each 3D image is composed of 40 z stacks of images recorded with 1 μm resolution in depth. The z stacks of images are loaded in the 3D object counter plug-in of IMAGE J. The cluster volumes are normalized by

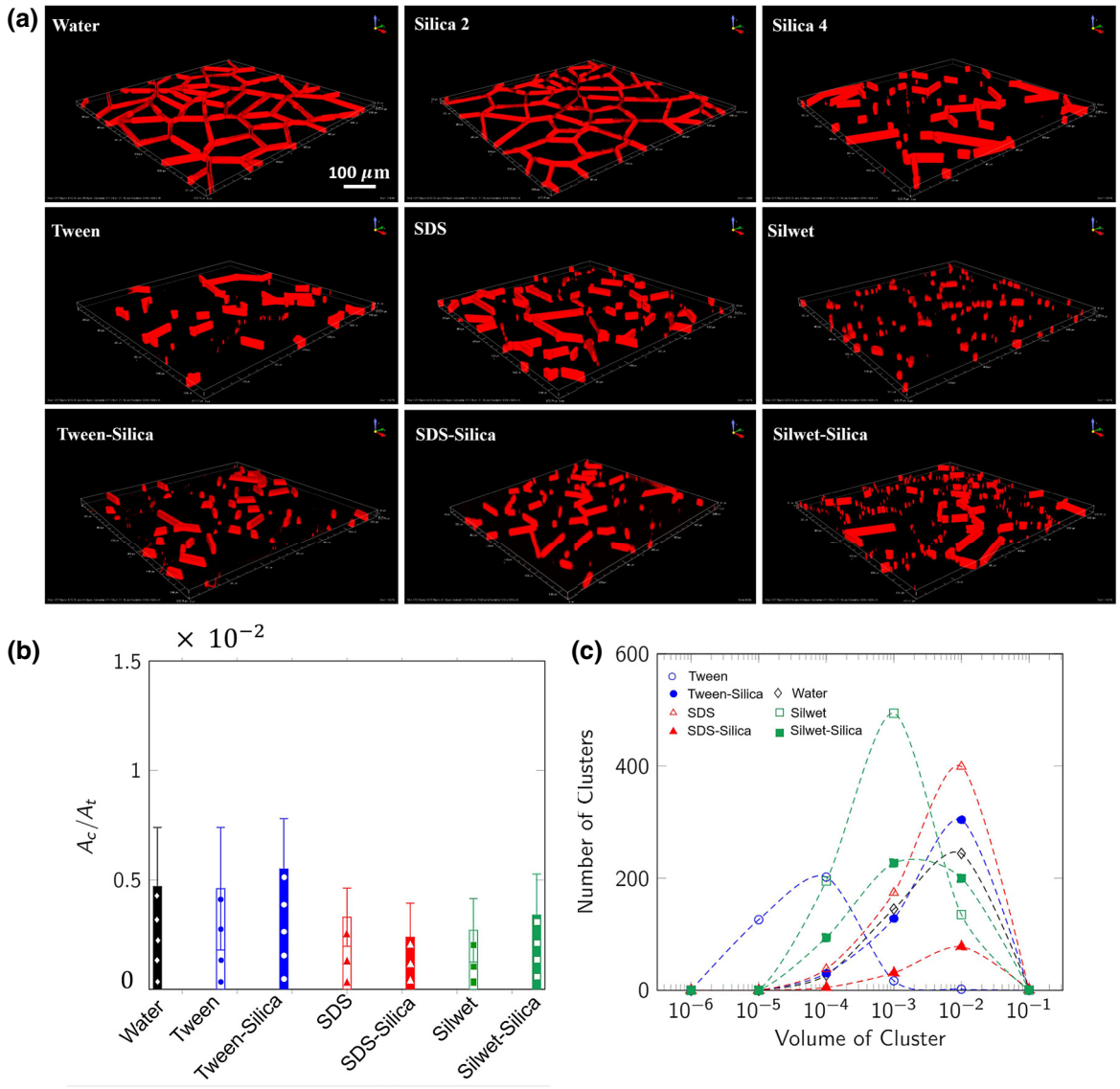

FIG. 6. The two-phase flow in the presence of nanoparticles and surfactants in nonwetting solution. (a) 3D views of the remaining oil inside the micromodel at $t_d = 10$ [$t_d = (Q_{\text{inj}}t)/V$] for water, Silica 2, Silica 4, surfactants, and surfactant-silica suspensions. The continuous oil phase in water flooding changes to clusters of oil blobs in the presence of surfactants. The size and number of oil clusters are dependent on the type of surfactant. Compared to other flooding scenarios, Silwet surfactant results in a larger number of tiny oil droplets and a higher sweep efficiency. Silica 2 and Silica 4 show different patterns where the wetting phase is mainly continuous in Silica 2, but seems broken in Silica 4. (b) Dimensionless average cluster size for water and different surfactant solutions. Silwet and SDS are stronger in decreasing the cluster size than water and Tween. (c) Dimensionless cluster volume distribution for water and different surfactant solutions.

the micromodel pore volume and categorized in six bins [0.000001, 0.01]. Figure 6(c) illustrates the distribution of cluster volumes for water (black), Tween (blue), SDS (red), Silwet (green), and their combinations with 2 wt. % silica nanoparticles. Silica shows a two-fold effect. It shifts the cluster volumes toward larger bins. The shift is negligible for SDS while it is considerable for Tween. There is also a reduction in the overall number of oil clusters when silica is added, although the change is not obvious for Tween. Please note that for Tween, unlike other cases, the clusters of residual wetting phase are mainly located at the microchannel intersections. In the last section of this paper, we closely examine the wetting state of a microchannel, which may influence the viscous phase distribution.

The cluster shapes are quantified using 3D, ×10 magnification images (1.16 μm/pixel and 1 μm/pixel resolutions in the horizontal plane and depth, respectively). We classify the clusters into two groups (spherical and nonspherical) based on their shape factor. The shape factor is evaluated as the ratio of cluster surface area to its

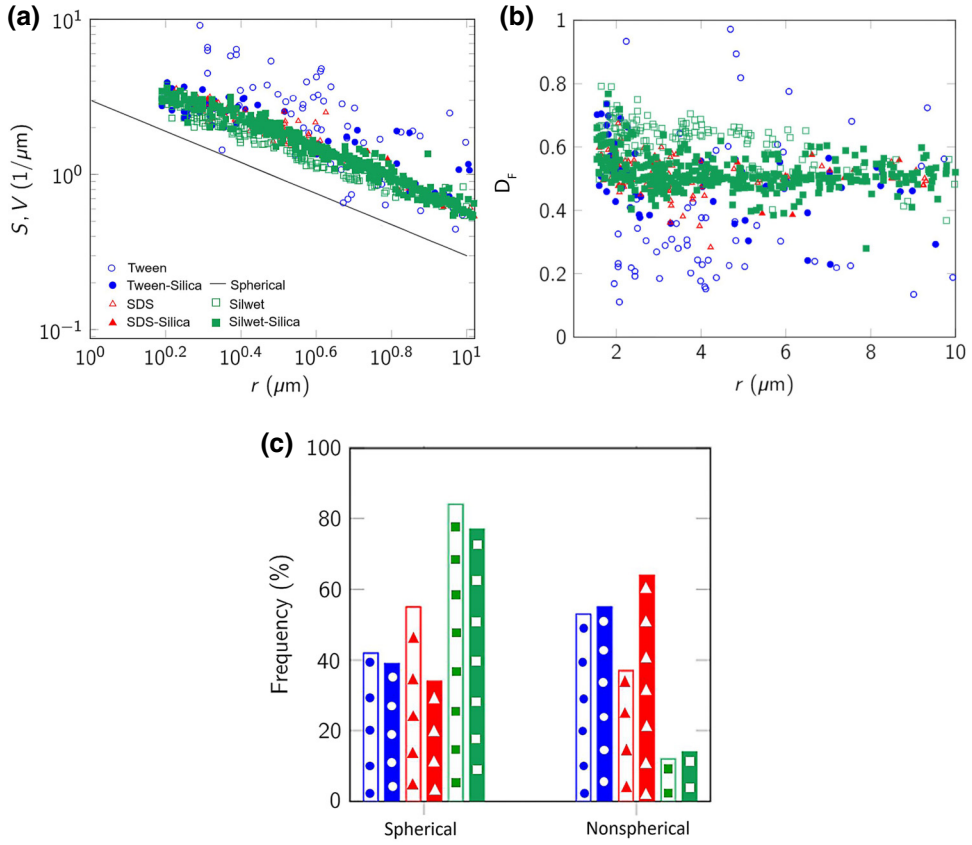

FIG. 7. (a) The cluster shape factor (surface area to volume ratio). r is the equivalent radius of clusters assuming that they are spheres. The solid line shows the shape factor of a perfect sphere$(3/r)$. (b) Deviation factor indicating how close the clusters are to perfect spheres when $D_F = 1$. Clusters with $D_F > 0.5$ are considered as spherical clusters. (c) Cluster classification based on the shape factor is divided into two groups, spherical and nonspherical.

volume (S/V) which is $(3/r)$ for a perfect sphere with the radius of r. Figure 7(a) is the plot of cluster shape factors as a function of equivalent spherical radius r. The plot shows the deviation of the cluster shape factors from that of a sphere (shown with a solid black line), i.e., the degree of spheroidicity. The clusters in our micromodels are mainly in the form of rectangular cuboids and capsules, and thus the shape factors are larger than the sphere one. In order to distinguish the effect of nanoparticles on the shape factor, we plot the ratio of shape factor for an equivalent sphere to that of the cluster $D_F = (3/r)/(S/V)$ as a function of equivalent radius r. D_F is a coefficient between zero and one characterizing the cluster shapes as shown in Fig. 7(b). As cluster shapes become closer to spheres, D_F values approach one. Overall, when silica is added to the displacing phase, D_F gets smaller signaling that the clusters are further deviated from perfect spheres. Here, we classify clusters that have $D_F > 0.5$ as spherical clusters, and clusters with a diameter larger than $15\,\mu$m and $D_F < 0.5$ as nonspherical ones. Figure 7(c) shows the cluster distribution in spherical and nonspherical groups. Adding silica to the surfactant solutions consistently decreases the number of spherical clusters and increases the number of the nonspherical clusters.

D. Phase interferences: the roles of silica and surfactants

The shape and number of fluid-fluid interfaces in the flow of immiscible fluids in porous media can provide insight into the phase interactions and fluid distributions. The number and area of interfaces are characterized either by the specific interfacial area or the quantity of wetting and nonwetting phase clusters (blobs). Different imaging systems have been used to characterize the properties of interfaces under a static condition; however, capturing the dynamic of interfaces requires a more precise and faster experimental technique [52]. Microfluidics provides an excellent opportunity for real-time visualization and tracing of fluid-fluid interfaces [53,54]. Historically, the number and curvature of fluid interfaces have been used to quantify the dynamics of immiscible displacement in the absence of chemical additives [45,46]. The presence of surface-active agents and particles is common in underground flow processes and influence the dynamics of two

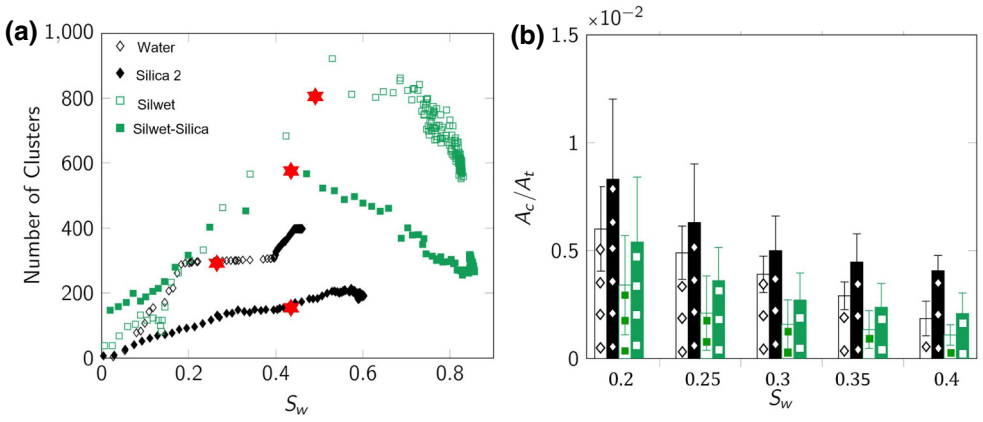

FIG. 8. The number of clusters and average cluster size as a function of aqueous phase saturation. (a) The number of clusters (the fluid-fluid interface representatives) as a function of aqueous phase saturation. All measurements are done until $t_d = 5$. (b) The average cluster size [area of the cluster (A_c)/total area of the microchannel (A_t)] as a function of aqueous phase saturation. The error bars indicate the standard deviation for each experiment.

phase flows and patterns of wetting phase distribution. In this section, we use the concept of phase interferences to quantify the influence of each chemical additive (surfactants and nanoparticles) on the fluid dynamics and viscous wetting phase mobilization. This is achieved by conducting experiments that evaluate the number of wetting phase clusters at different time scales.

The wetting phase (oil) clusters are counted, indicating the number of interfaces, as a function of the aqueous phase saturation [Fig. 8(a)] for water, Silica 2 (a representation of silica solutions), Silwet (a representation of nonionic surfactant solutions), and a Silwet-Silica mixture. There is an abrupt increase in the number of clusters for each setting until t_{BT}. At this point, the number of clusters is dependent on the type of displacing fluid used: 300 for water, 600 for Silwet-silica, and 800 for Silwet. The number of clusters after the breakthrough time depends on the balance between the generation and production of clusters. Post injection of water (after t_{BT}) results in a slow rise in the number of clusters and indicates (i) a bypass of large oil ganglia and (ii) an invasion of a few new microchannels. Thus, additional mobilized ganglia are formed. During Silwet and Silwet-Silica flooding the number of clusters decreases over time as the injection continues to signal the appearance of small oil blobs (Fig. 6). The oil disintegration is outbalanced by the number of wetting phase blobs, displaced toward the production port. Hence, the number of oil clusters decreases over time, reaching less than 600 for Silwet.

One can conclude that the rates of mobilization and removal of the viscous oil are strongly associated with how effectively a flooding fluid disintegrates the continuous viscous oil phase. The rates of mobilization and removal are highest for Silwet. The addition of 2 wt. % silica in water and surfactant solutions decreases the number of clusters throughout the process in flow experiments without silica. This implies that the placement of silica nanoparticles at the oil-water interfaces forms a rigid interface requiring more energy to be broken down [55]. The effect is lower for clusters that are larger in size. Figure 6 represents the impact of silica nanoparticles on the number of clusters. When silica nanoparticles are added to the Silwet solution, larger clusters are generated in the remaining oil.

The mean size of clusters (the remaining oil blobs) is measured at different saturations for each experiment, scaled by the total area of the channel network [Fig. 8(b)]. In each experiment, there is an abrupt decline in the mean cluster size before reaching $S_w = 0.2$. The size of the cluster remains unchanged in aqueous phase saturations higher than $S_w = 0.4$. The average cluster size is plotted against the aqueous phase saturation in the range of $0.2 < S_w < 0.4$ for water, Silica 2, Silwet, and Silwet-Silica [Fig. 8(b)]. The error bars represent the standard deviation of the cluster size. The Silwet flooding results in a smaller cluster size than does the water flooding. For instance, the average cluster size for the Silwet flooding for $S_w = 0.4$ is about 2.5 times smaller than that of the water flooding. Smaller clusters flow more easily through the microchannels enhancing the viscous oil removal from the fluidic network. The addition of 2 wt. % silica nanoparticles to water and Silwet solutions increases the average cluster size of the wetting phase by about 40% and 60%, respectively.

The size distribution of clusters scaled by the total surface area of the microchannel is plotted in six bins, at a representative saturation of $S_w = 0.25$ [Fig. 9(a)]. The size distribution of the clusters demonstrates an obvious shift in the maximum number and minimum size of clusters from Silwet to Silwet-Silica flooding and from water to Silica 2 flooding. Similar trends in the size distribution of clusters are observed for the saturation in the range of $0.2 < S_w < 0.4$.

The most frequently occurring cluster size (mode) is determined using an analysis of the experimental images. Figure 9(b) presents the mode for all flooding scenarios examined in Fig. 9(a) at saturations ranging from $0 < S_w < 0.4$. The modes for the water and silica floodings remain limited within the bin thresholds of (0.0002, 0.001), while the modes for the Silwet and Silwet-silica floodings remain limited within the bin thresholds of (0.00004, 0.002). The

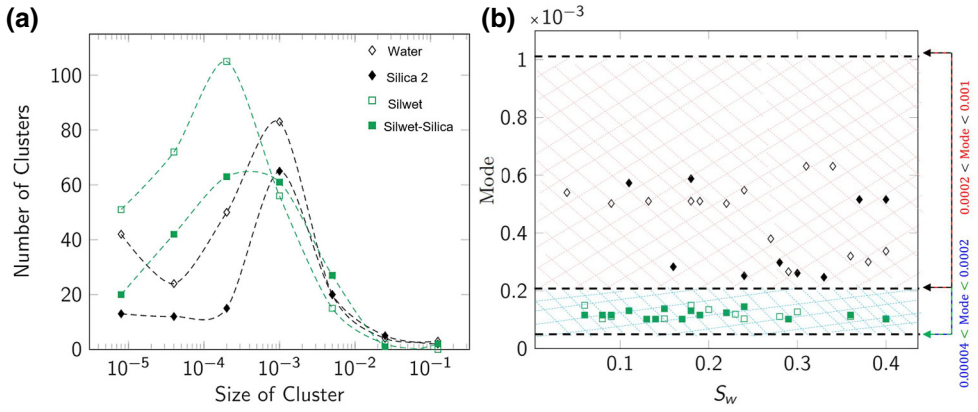

FIG. 9. Statistical analysis of the cluster size. (a) The scaled size distribution of clusters at $S_w = 0.25$. The curves are only a fit to the data points and are meant to be visual guides for eyes. (b) The most frequently occurring cluster size (mode) as a function of the aqueous phase saturation.

mode values decrease in the presence of Silwet surfactant, which is directly related to the reduction in IFT. The incorporation of silica nanoparticles increases the average cluster sizes, but it does not change the mode values. The mode values remain nearly unchanged in response to the increase in the Silwet and Silwet-Silica saturation.

E. The status of the remaining oil clusters with respect to the solid and aqueous phases

We examine the 3D images (after the displacement) to evaluate the status of clusters in terms of attachment to the wall. The analysis reveals that clusters remain connected to the channel walls once the flow ceases. Figure 10 depicts the clusters in one intersection in the selected z stacks (at the depths of 0, 5, 10, 15, and 20 μm) for three cases of water, Silica 4, and Silwet. It is evident that clusters are partially or totally in depth attached to the wall. Please note that the micromodel is made of hydrophobic PDMS, and thus one may expect to see an affinity of the surface to the oil phase.

Hydrophobic microchannels are used to perform the multiphase flow experiments in this work. The interface between the viscous oil (wetting phase) and the aqueous phase in the two-phase flow experiments is expected to be concave toward the oil phase (Fig. 11). The shape of the interface is concave toward the aqueous phase in the presence of Tween surfactant. This may be due to the adsorption of Tween surfactant at the solid surface. Interestingly, the addition of silica nanoparticles into the Tween solution flattens the shape of the interface, which can be a direct consequence of reducing surfactant adsorption on the solid surfaces [56,57]. Further analysis is required to investigate the effect of silica nanoparticles on the reduction of surfactant adsorption volume from the solid surface.

The influence of interfacial materials on the dynamics of fluid displacement is mainly studied for low viscous fluids using static experiments with micromodels and core scale models coupled with bulk emulsion stability tests [58–61]. Previous multiphase flow studies in dynamic conditions using single oil drop displacement by nanofluids on a flat surface and within capillary tubes have shown that nanoparticles are effective in the removal of oil films from the substrate [18,62,63] and oil displacement through porous media [19,64]. A combination of nanoparticles and wetting agents (mostly SDS) has been effective since SDS (anionic) micellar solution has a decent wetting performance on silica-type surfaces compared to other ionic or nonionic micellar solutions. Other types of nanofluids such as silica and polymeric nanoparticles have been utilized for oil displacement investigations [65] where the observed phenomena show the efficiency of nanoparticles combined with wetting agents. The interfacial tension between the oil and nanofluid reported in the literature is determined to be below 20 mN/m and the oil films are removed from hydrophilic surfaces in micellar solutions. Moreover, there are a few experiments focusing on the dynamics of viscous fluid interactions with an aqueous phase. Recently, the role of oil viscosity on the dewetting dynamics of a viscous oil by water was characterized [66]. In another work, the deformation of a viscous oil-aqueous phase interface was captured and analyzed using 2D images of Hele-Shaw cell experiments [67]. Despite the extensive applications of nanoparticles and surfactant-laden interfaces in two-phase flow systems, the exact effect of each nanoparticle and surfactants on the size and number of wetting and nonwetting clusters, especially for a viscous wetting phase, has not been reported.

This work reports the detailed 3D analysis of the effect of interfacial materials on the fluid-fluid interfaces in a dynamic condition. The fluid-fluid and fluid-solid interactions are characterized by the magnified 3D images of the multiphase flow process within micromodels. The characterization reveals viscous oil is mobilized differently in the presence of nanoparticles and surfactants within the microscale channels. Following the water injection, a thick layer (up to 40% of the microchannel height) of the wetting phase (oil) remains on many microchannel walls. The removal of oil films from hydrophobic substrates is characterized by incorporating silica nanoparticle solutions without using wetting agents. The results show that a high concentration of silica nanoparticles assist the

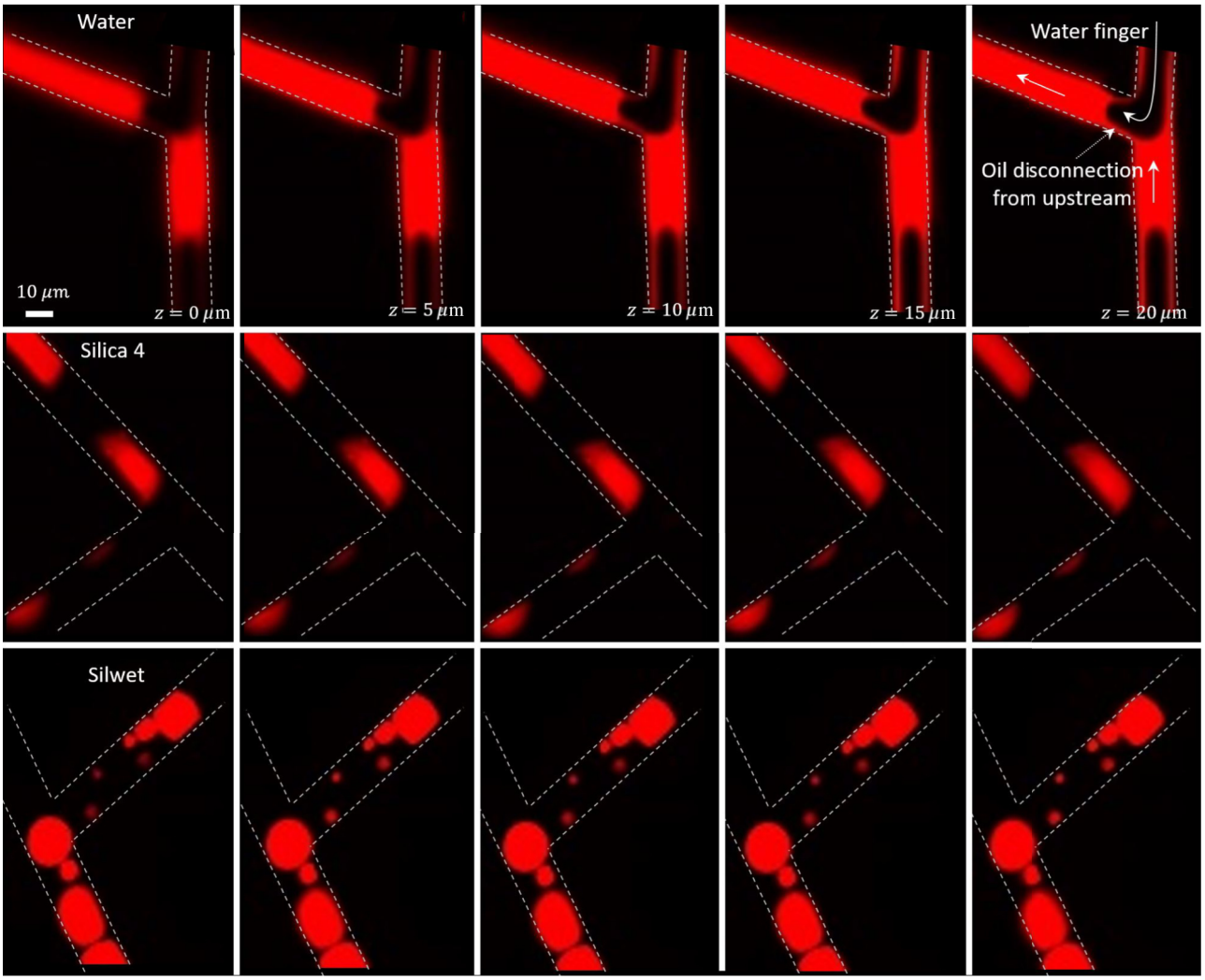

FIG. 10. ×20 magnification of z stack images of the microchannel after 10 pore volume injected (PVI) for water, Silica 4, and Silwet. Images are presented at $z = 0,\ 5, 10, 15$, and 20 μm. This figure shows that the reaming oil clusters are mainly attached to the walls of the micromodel. The solid white arrow in the top right corner figure shows the direction of flow and how the wetting phase is breaking at the intersection.

effective removal of the oil film from hydrophobic surfaces [19]. When adding silica nanoparticles, the thickness of the remaining oil decreases to zero at 4 wt.% silica concentrations. In the vicinity of the three phase contact line, nanoparticles place themselves in a layering structure creating the required disjoining pressure for the oil film [18].

The results demonstrate that the mechanism of wetting phase displacement in the presence of surfactants is dominated by breaking the remaining wetting phase into smaller droplets. This mechanism facilitates the oil movement toward the outlet port and increases the volume of wetting phase production. In Silwet flooding, the continuous oil phase turns into many tiny droplets that are easily transported by the carrier solution. Silwet is a nonionic surfactant with an immense ability to alter wettability, and thus it can displace the oil phase from hydrophobic surfaces more readily than other surfactants [68]. Silwet has a lower HLB (around 10) compared to other water-soluble surfactants (40 for SDS) [69]. Silwet molecules are initially dispersed in the water phase and once injected into the micromodel and in contact with the oil phase, they place their hydrophobic portion into the oil phase as a result of a higher affinity of Silwet molecules for transferring from the bulk to the interface compared to the SDS and Tween. The Silwet vigorously disturbs the interface creating a higher number of smaller droplets. Moreover, we find that increasing the aqueous phase saturation and adding silica to the displacing phase do not alter the most frequently occurring cluster size for water and Silwet.

Please note that the micromodel consists of cross-sectionally monosized channels. Thus, the oil-phase

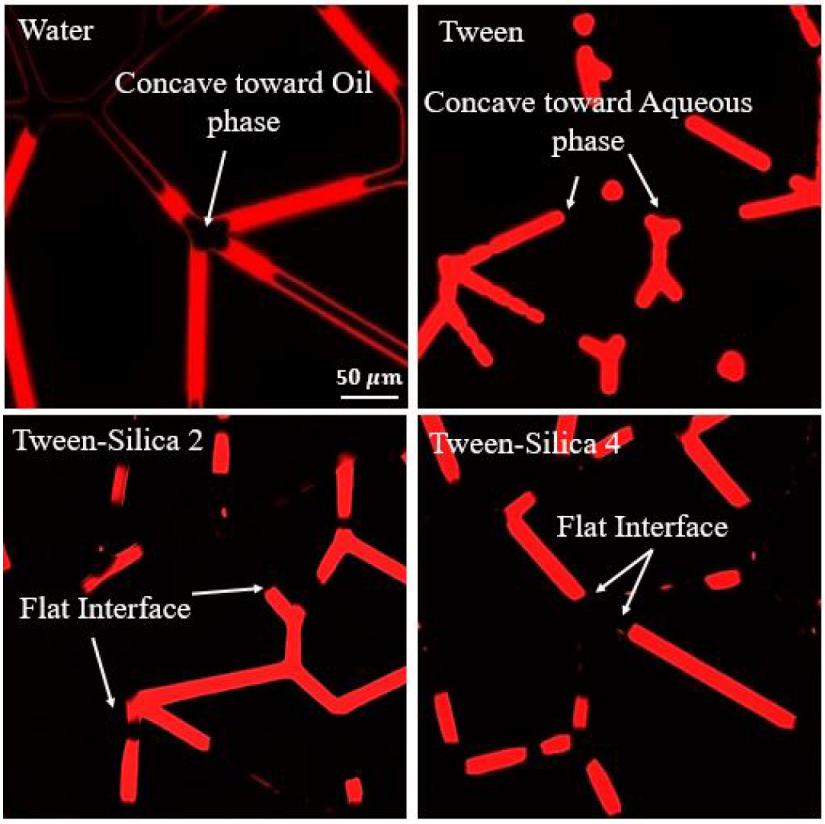

FIG. 11. The shape of the interfaces between the viscous oil (wetting phase) and different nonwetting solutions. The interface is concave toward the oil at the water-oil interface. However, the shape of the interface changes to concave toward the aqueous phase in the presence of Tween surfactants. The addition of 2 and 4 wt. % silica to Tween flattens the interface.

fragmentation mechanisms driven by the microscale heterogeneities (i.e., snap-off in constricted capillaries), or the by-passed phase trappings due to the multisized area open to flow, are absent in the present model. There are two chief mechanisms contributing to the breaking of the wetting phase into smaller ganglia: wetting phase fragmentation at the channel junctions and the wetting film detachment. The micromodel has more than 1600 channel intersections. There are many occasions during which a stream of aqueous phase reaches an intersection that is full of oil. Thus, two streams of oil and water compete in entering the junction. However, as the aqueous phase has a higher mobility than the wetting phase, it breaks the stream of oil. For example, Fig. 10 depicts the advanced finger of the aqueous phase (from the top channel) that intrudes into the oil at the junction. The finger ultimately disconnects the oil phase in the downstream channel (on the left) from the rest of the phase in the upstream feeding channel (the bottom channel). This process continues until the oil from the feeding channel is displaced by the aqueous phase through the intersection. The wetting phase gets trapped in the feeding channels when the aqueous phase connects the inlet and outlet of those channels. The type and the size of the oil ganglia depend on the viscosity ratio of two liquids and the interfacial tension between the phases. This breaking mechanism gets intensified in the presence of surfactants. Please see the Supplemental Material at (URI) for the oil displacement and fragmentation by the Silwet solution (Movie S2) [47]. The second mechanism is related to the dewetting process of the channel walls. The intruding finger of the displacing fluid leaves behind a layer of wetting phase attached to the channel walls. The oil film length gradually shrinks from the rupture points and forms an oil blob as depicted in Fig. 5(b) for the case of Silica 4.

The phase interference concept is used to analyze fluid-fluid interfacial parameters. The fluid-fluid interference is quantified by the number of wetting phase clusters (blobs) as a function of aqueous phase saturation. It is determined that the number of oil clusters is an increasing function of saturation for representative water, Silica 2, Silwet, and Silwet-Silica flooding until the breakthrough time. Before the breakthrough time, the oil phase is recovered from the main flow stream while small clusters of oil remain stationary within the microchannels. Following the breakthrough time, the majority of the oil is produced from the small clusters suspended in the microchannels, hence the number of clusters decreases over time. Adding silica to Silwet solutions consistently decreases the number of oil clusters while increasing their sizes. The placement of silica nanoparticles in the vicinity of the oil-water interface results in the formation of stable oil-water interfaces requiring higher energy for break up. This observation is similar to the data in the literature on the effect of nanoparticles on the stability of oil-water emulsions [70]. Our results provide evidence for an open-ended discussion on the higher stability of nanoparticle-stabilized emulsions

than surfactant-stabilized emulsions due to their high thermal energy and the tendency to be pinned to the oil-water interface [55]. The nanoparticles stay longer at the interface as they require greater energy for detachment.

IV. SUMMARY AND CONCLUSION

In this paper, a series of multiphase flow analyses are implemented in microscale channels to examine the efficiency of viscous oil mobilization and displacement by an immiscible aqueous phase. Three-dimensional (3D) confocal images are captured to quantitatively evaluate the physical mechanisms underlying the displacement of the viscous wetting phase in microscale channels in the presence of surfactants, silica nanoparticles, and their combinations. Four different types of displacing fluids are examined to displace the heavy oil sample (viscosity of 178 mPa s). The overall displacement efficiency is found to be an increasing function of silica particles' concentration. There is an optimum silica concentration (2 wt. % in this study) and once above this, the incremental removal of the viscous oil is minor. The addition of anionic (SDS) and nonionic (Tween) surfactants enhances the wetting phase displacement from that of water. The maximum sweep efficiency is achieved using the employment of Trisiloxane surfactant (Silwet).

The fluid-fluid and fluid-solid interactions are characterized by means of a transparent and hydrophobic microfluidic-based microreservoir. Magnified 3D images of the multiphase flow process reveal that the viscous oil becomes mobilized differently in the presence of silica and surfactants within microscale channels. Following the water injection, a thick layer of oil remains on the channel walls. The viscous oil displacement in the presence of surfactants is governed by breaking the oil phase into smaller parts, which facilitates their movement toward the outlet port. During Silwet flooding, the continuous oil phase turns into many tiny droplets that are easily transported via the carrier solution. The results of this experimental study provide insight into mechanisms underlying the interaction of oil and the displacing fluid in the overall performance of a high viscous oil mobilization. This should guide further experiments to differentiate the effects of different parameters involved in multiphase flows with large viscosity contrast within micromodels.

ACKNOWLEDGMENTS

We acknowledge the support in part by SENER-CONACYT-Hidrocarburos program (project 280816) administered by Consejo Nacional de Ciencia y Tecnologia (CONACYT, Mexico), Natural Sciences and Engineering Council of Canada (NSERC), CMC Canadian Microsystem, and Canada Research Chair. The authors also gratefully acknowledge infrastructure funding from Canadian Foundation for Innovation (CFI).

[1] S. Berg, H. Ott, S. A. Klapp, A. Schwing, R. Neiteler, N. Brussee, A. Makurat, L. Leu, F. Enzmann, and J.-O. Schwarz, Real-time 3D imaging of Haines jumps in porous media flow, Proc. Natl. Acad. Sci. U.S.A. **110**, 3755 (2013).

[2] P. B. Kelemen and J. Matter, In situ carbonation of peridotite for CO_2 storage, Proc. Natl. Acad. Sci. U.S.A. **105**, 17295 (2008).

[3] S. Krevor, M. J. Blunt, S. M. Benson, C. H. Pentland, C. Reynolds, A. Al-Menhali, and B. Niu, Capillary trapping for geologic carbon dioxide storage–from pore scale physics to field scale implications, Int. J. GreenH. Gas Con. **40**, 221 (2015).

[4] T. Pak, I. B. Butler, S. Geiger, M. I. van Dijke, and K. S. Sorbie, droplet fragmentation: 3D imaging of a previously unidentified pore-scale process during multiphase flow in porous media, Proc. Natl. Acad. Sci. U.S.A. **112**, 1947 (2015).

[5] Z. Wang, C. Wang, and K. Chen, Two-phase flow and transport in the air cathode of proton exchange membrane fuel cells, J. Power Sources **94**, 40 (2001).

[6] J. W. Mercer and R. M. Cohen, A review of immiscible fluids in the subsurface: Properties, models, characterization and remediation, J. Contam. Hydrol. **6**, 107 (1990).

[7] J. Sheng, *Modern Chemical Enhanced Oil Recovery: Theory and Practice* (Gulf Professional Publishing, 2010).

[8] S. Thomas, S. Ali, J. Scoular, and B. Verkoczy, Chemical methods for heavy oil recovery, J. Can. Petrol Technol. **40** (2001).

[9] S. Kumar, P. Panigrahi, R. K. Saw, and A. Mandal, Interfacial interaction of cationic surfactants and its effect on wettability alteration of oil-wet carbonate rock, Energy Fuels **30**, 2846 (2016).

[10] M. Mirzaei, D. A. DiCarlo, and G. A. Pope, Visualization and analysis of surfactant imbibition into oil-wet fractured cores, SPE J. **21**, 101 (2016).

[11] S. Strand, T. Puntervold, and T. Austad, Water based EOR from clastic oil reservoirs by wettability alteration: A review of chemical aspects, J. Petrol. Sci. Eng. **146**, 1079 (2016).

[12] G. Cheraghian and L. Hendraningrat, A review on applications of nanotechnology in the enhanced oil recovery part B: Effects of nanoparticles on flooding, Int. Nano Lett. **6**, 1 (2016).

[13] X. Sun, Y. Zhang, G. Chen, and Z. Gai, Application of nanoparticles in enhanced oil recovery: A critical review of recent progress, Energies **10**, 345 (2017).

[14] R. Crane and T. Scott, Nanoscale zero-valent iron: Future prospects for an emerging water treatment technology, J. Hazard. Mater. **211**, 112 (2012).

[15] H. Ehtesabi, M. M. Ahadian, V. Taghikhani, and M. H. Ghazanfari, Enhanced heavy oil recovery in sandstone cores using TiO_2 nanofluids, Energy Fuels **28**, 423 (2013).

[16] Y. H. Shokrlu and T. Babadagli, Viscosity reduction of heavy oil/bitumen using micro-and nano-metal particles during aqueous and non-aqueous thermal applications, J. Petrol. Sci. Eng. **119**, 210 (2014).

[17] G. Cheraghian and L. Hendraningrat, A review on applications of nanotechnology in the enhanced oil recovery part A: Effects of nanoparticles on interfacial tension, Int. Nano Lett. **6**, 129 (2016).
[18] D. T. Wasan and A. D. Nikolov, Spreading of nanofluids on solids, Nature **423**, 156 (2003).
[19] H. Zhang, T. Ramakrishnan, A. Nikolov, and D. Wasan, Enhanced oil displacement by nanofluid's structural disjoining pressure in model fractured porous media, J. Colloid Interface Sci. **511**, 48 (2018).
[20] R. Li, P. Jiang, C. Gao, F. Huang, R. Xu, and X. Chen, Experimental investigation of silica-based nanofluid enhanced oil recovery: The effect of wettability alteration, Energy Fuels **31**, 188 (2016).
[21] Y. Li, C. Dai, H. Zhou, X. Wang, W. Lv, Y. Wu, and M. Zhao, A novel nanofluid based on fluorescent carbon nanoparticles for enhanced oil recovery, Ind. Eng. Chem. Res. **56**, 12464 (2017).
[22] D. Luo, F. Wang, J. Zhu, F. Cao, Y. Liu, X. Li, R. C. Willson, Z. Yang, C.-W. Chu, and Z. Ren, Nanofluid of graphene-based amphiphilic janus nanosheets for tertiary or enhanced oil recovery: High performance at low concentration, Proc. Natl. Acad. Sci. U.S.A. **113**, 7711–7716 (2016).
[23] K. Y. Yoon, H. A. Son, S. K. Choi, J. W. Kim, W. M. Sung, and H. T. Kim, Core flooding of complex nanoscale colloidal dispersions for enhanced oil recovery by in situ formation of stable oil-in-water pickering emulsions, Energy Fuels **30**, 2628 (2016).
[24] N. S. K. Gunda, B. Bera, N. K. Karadimitriou, S. K. Mitra, and S. M. Hassanizadeh, Reservoir-on-a-chip (ROC): A new paradigm in reservoir engineering, Lab Chip **11**, 3785 (2011).
[25] C. A. Reynolds, H. Menke, M. Andrew, M. J. Blunt, and S. Krevor, Dynamic fluid connectivity during steady-state multiphase flow in a sandstone, Proc. Natl. Acad. Sci. U.S.A. **114**, 8187 (2017).
[26] Y. Zhang, A. Sanati-Nezhad, and S. Hejazi, Geo-material surface modification of microchips using layer-by-layer (LbL) assembly for subsurface energy and environmental applications, Lab Chip **18**, 285 (2018).
[27] A. Anbari, H. T. Chien, S. S. Datta, W. Deng, D. A. Weitz, and J. Fan, Microfluidic model porous media: Fabrication and applications, Small **14**, 1703575 (2018).
[28] J. Murison, B. Semin, J.-C. Baret, S. Herminghaus, M. Schröter, and M. Brinkmann, Wetting Heterogeneities in Porous Media Control Flow Dissipation, Phys. Rev. Appl. **2**, 034002 (2014).
[29] J. M. Campbell, D. Ozturk, and B. Sandnes, Gas-Driven Fracturing of Saturated Granular Media, Phys. Rev. Appl. **8**, 064029 (2017).
[30] Z. Zhang, T. Kong, C. Zhou, and L. Wang, Engineering the Flow of Liquid Two-Phase Systems by Passive Noise Control, Phys. Rev. Appl. **9**, 024036 (2018).
[31] B. Bao, J. Riordon, F. Mostowfi, and D. Sinton, Microfluidic and nanofluidic phase behaviour characterization for industrial CO_2, oil and gas, Lab Chip **17**, 2740 (2017).
[32] T.s.E. Chávez-Miyauchi, A. Firoozabadi, and G. G. Fuller, Nonmonotonic elasticity of the crude oil–brine interface in relation to improved oil recovery, Langmuir **32**, 2192 (2016).
[33] V. A. Lifton, Microfluidics: An enabling screening technology for enhanced oil recovery (EOR), Lab Chip **16**, 1777 (2016).
[34] Q. Zhang and S. M. Hassanizadeh, The role of interfacial tension in colloid retention and remobilization during two-phase flow in a polydimethylsiloxane micro-model, Chem. Eng. Sci. **168**, 437 (2017).
[35] G. Cheraghian, S. Kiani, N. N. Nassar, S. Alexander, and A. R. Barron, Silica nanoparticle enhancement in the efficiency of surfactant flooding of heavy oil in a glass micromodel, Ind. Eng. Chem. Res. **56**, 8528 (2017).
[36] J. Cui and T. Babadagli, Use of new generation chemicals and nano materials in heavy-oil recovery: Visual analysis through micro fluidics experiments, Colloid Surf. A Physicochem. Eng. Asp. **529**, 346 (2017).
[37] P. Nguyen, H. Fadaei, and D. Sinton, Pore-scale assessment of nanoparticle-stabilized CO_2 foam for enhanced oil recovery, Energy Fuels **28**, 6221 (2014).
[38] K. Xu, P. Zhu, C. Huh, and M. T. Balhoff, Microfluidic investigation of nanoparticles' role in mobilizing trapped oil droplets in porous media, Langmuir **31**, 13673 (2015).
[39] P. Bazazi, I. D. Gates, A. Sanati Nezhad, and S. H. Hejazi, in SPE Canada Heavy Oil Technical Conference (Society of Petroleum Engineers, 2017).
[40] P. Bazazi, A. Sanati-Nezhad, and S. H. Hejazi, Role of chemical additives on water-based heavy oil mobilization: A microfluidic approach, Fuel (unpublished).
[41] S. S. Datta, J.-B. Dupin, and D. A. Weitz, Fluid breakup during simultaneous two-phase flow through a three-dimensional porous medium, Phys. Fluids **26**, 062004 (2014).
[42] S. S. Datta, T. Ramakrishnan, and D. A. Weitz, Mobilization of a trapped non-wetting fluid from a three-dimensional porous medium, Phys. Fluids **26**, 022002 (2014).
[43] R. Singh and K. K. Mohanty, Foam flow in a layered, heterogeneous porous medium: A visualization study, Fuel **197**, 58 (2017).
[44] Y. Edery, D. Weitz, and S. Berg, Surfactant Variations in Porous Media Localize Capillary Instabilities During Haines Jumps, Phys. Rev. Lett. **120**, 028005 (2018).
[45] M. Wu, F. Xiao, R. M. Johnson-Paben, S. T. Retterer, X. Yin, and K. B. Neeves, Single-and two-phase flow in microfluidic porous media analogs based on voronoi tessellation, Lab Chip **12**, 253 (2012).
[46] C. A. Schneider, W. S. Rasband, and K. W. Eliceiri, NIH image to ImageJ: 25 years of image analysis, Nat. Methods **9**, 671 (2012).
[47] See Supplemental Material at http://link.aps.org/supplemental/10.1103/PhysRevApplied.11.014042 for the details of materials, microchip fabrication, and properties of oil and aqueous phases (interfacial tension and three-phase contact angle data).
[48] A. Maghzi, A. Mohebbi, R. Kharrat, and M. H. Ghazanfari, Pore-scale monitoring of wettability alteration by silica nanoparticles during polymer flooding to heavy oil in a five-spot glass micromodel, Transport Porous Med. **87**, 653 (2011).
[49] A. Nikolov, K. Kondiparty, and D. Wasan, Nanoparticle self-structuring in a nanofluid film spreading on a solid surface, Langmuir **26**, 7665 (2010).

[50] D. Wasan, A. Nikolov, and K. Kondiparty. The wetting and spreading of nanofluids on solids: Role of the structural disjoining pressure. Curr. Opin. Colloid Interface Sci. **16**, 344 (2011).

[51] P. D. Fletcher, L. D. Savory, A. Clarke, and A. M. Howe, Model study of enhanced oil recovery by flooding with aqueous solutions of different surfactants: How the surface chemical properties of the surfactants relate to the amount of oil recovered, Energy Fuels **30**, 4767 (2016).

[52] P. Chen, L. Jiang, and D. Han, In situ imaging of multiphase bio-interfaces at the micro-/nanoscale, Small **7**, 2825 (2011).

[53] N. Karadimitriou, S. Hassanizadeh, V. Joekar-Niasar, and P. Kleingeld, Micromodel study of two-phase flow under transient conditions: Quantifying Effects of Specific Interfacial Area, Water Resour. Res. **50**, 8125 (2014).

[54] V. Joekar-Niasar, S. M. Hassanizadeh, and H. Dahle, Non-equilibrium effects in capillarity and interfacial area in two-phase flow: Dynamic pore-network modelling, J. Fluid Mech. **655**, 38 (2010).

[55] B. P. Binks, Particles as surfactants—Similarities and differences, Curr. Opin. Colloid Interface Sci. **7**, 21 (2002).

[56] Y. Wu, W. Chen, C. Dai, Y. Huang, H. Li, M. Zhao, L. He, and B. Jiao, Reducing surfactant adsorption on rock by silica nanoparticles for enhanced oil recovery, J. Petrol. Sci. Eng. **153**, 283 (2017).

[57] E. Nourafkan, Z. Hu, and D. Wen, Nanoparticle-Enabled Delivery of Surfactants in Porous Media, J. Colloid Interface Sci. **519**, 44–57 (2018).

[58] S. Maaref, S. Ayatollahi, N. Rezaei, and M. Masihi, The effect of dispersed phase salinity on water-in-oil emulsion flow performance: A micromodel Study, Ind. Eng. Chem. Res. **56**, 4549 (2017).

[59] H. Pei, G. Zhang, J. Ge, J. Zhang, and Q. Zhang, Investigation of synergy between nanoparticle and surfactant in stabilizing oil-in-water emulsions for improved heavy oil recovery, Colloid Surf. A Physicoch. Eng. Asp. **484**, 478 (2015).

[60] S. Jones, V. Van Der Bent, R. Farajzadeh, W. Rossen, and S. Vincent-Bonnieu, Surfactant screening for foam EOR: Correlation between bulk and core-flood experiments, Colloid Surf. A Physicoch. Eng. Asp. **500**, 166 (2016).

[61] D. Luo, F. Wang, J. Zhu, F. Cao, Y. Liu, X. Li, R. C. Willson, Z. Yang, C.-W. Chu, and Z. Ren, Nanofluid of graphene-based amphiphilic janus nanosheets for tertiary or enhanced oil recovery: High performance at low concentration, Proc. Natl. Acad. Sci. U.S.A. **113**, 7711 (2016).

[62] S. Lim, H. Zhang, P. Wu, A. Nikolov, and D. Wasan, The dynamic spreading of nanofluids on solid surfaces–Role of the nanofilm structural disjoining pressure, J. Colloid Interface Sci. **470**, 22 (2016).

[63] S. Lim, H. Horiuchi, A. D. Nikolov, and D. Wasan, Nanofluids alter the surface wettability of solids, Langmuir **31**, 5827 (2015).

[64] H. Zhang, A. Nikolov, J. Feng, and D. Wasan, The dynamics of the annular liquid layer inside a cylindrical capillary, Phys. Fluids **28**, 024107 (2016).

[65] A. Nikolov and H. Zhang, The dynamics of capillary-driven two-phase flow: The role of nanofluid structural forces, J. Colloid Interface Sci. **449**, 92 (2015).

[66] P. Bazazi, A. Sanati-Nezhad, and S. H. Hejazi, Wetting dynamics in two-liquid systems: Effect of the surrounding phase viscosity, Phys. Rev. E **97**, 063104 (2018).

[67] S. Raza, S. H. Hejazi, and I. D. Gates, Two phase flow of liquids in a narrow gap: Phase interference and hysteresis, Phys. Fluids **28**, 074102 (2016).

[68] N. Kovalchuk, A. Trybala, O. Arjmandi-Tash, and V. Starov, Surfactant-enhanced spreading: Experimental achievements and possible mechanisms, Adv. Colloid Interface Sci. **233**, 155 (2016).

[69] Y. Zhang and F. Han, The spreading behaviour and spreading mechanism of new glucosamide-based trisiloxane on polystyrene surfaces, J. Colloid Interface Sci. **337**, 211 (2009).

[70] B. P. Binks and C. P. Whitby, Nanoparticle silica-stabilised oil-in-water emulsions: Improving emulsion stability, Colloid Surf. A Physicoch. Eng. Asp. **253**, 105 (2005).